Accelerated life testing study of a novel tidal turbine blade attachment

Oscar de la Torre[1,2*], Daithi Moore[4], Declan Gavigan[4], Jamie Goggins[1,2,3]
[1]Civil Engineering, College of Engineering and Informatics, National University of Ireland Galway, Galway, Ireland
[2]MaREI Centre for Marine and Renewable Energy, Galway, Ireland
[3]Ryan Institute for Environmental, Marine and Energy Research, Galway, Ireland
[4]OpenHydro, Greenore Port, Greenore, Co. Louth, Ireland
*corresponding author email address: jamie.goggins@nuigalway.ie; +353 91 49 2609

ABSTRACT: This paper describes the setup and some results of an accelerated life testing study of a tidal turbine blade attachment, which involved high-cycle fatigue testing of a tidal turbine subsystem at the Large Structure Laboratory of the National University of Ireland Galway (NUI Galway). Tidal turbines are in an early stage of development, which implies that there is no standard design and many different approaches are emerging in the market. The subsystem described in this paper is a 3/8 scaled down part of a 10-blade hubless turbine, developed by OpenHydro, a company specialising in the design, manufacture, installation, and maintenance of marine turbines generating renewable energy from tidal streams. The subsystem consists of a blade and a sector of the rotating ring. The sample was installed on an existing 10m x 6m x 6 m reconfigurable test frame and was loaded with a servo-hydraulic actuator controlled by an advanced software system, which allowed for an accurate sinusoidal load-controlled high-cycle fatigue test. The sample was loaded at four different levels to accumulate damage representative of a typical tidal turbine deployment life. The main objective of the test was to analyse the structural behaviour of the attachment system solution (blade-rotating ring) under fatigue load, particularly the internal structural welds, and to validate previously developed numerical models. To address all the requirements and to obtain valuable data, a large experimental test was set up. A total of 110 channels in a multi-channel data acquisition system were used to simultaneously acquire strain, displacement, and load data. Accurate measurements of temporal deformations and movement in a 3D field at the rear side of the ring were also acquired using a Digital Image Correlation system. The mechanism of failure was expected to be fatigue crack propagation at locations pre-determined in a structural analysis of the system.

KEY WORDS: Fatigue testing, Tidal turbine subsystem, Ocean engineering, Structural testing, Marine renewable energy.

1 INTRODUCTION

1.1 Background

Currently, the most urgent environmental impact that needs to be addressed in Europe is climate change as a result of 2020 targets for energy generation from renewable sources (Directive 2009/28/EC) and greenhouse gas emission reduction (Directive 2012/27/EU), along with the COP21 agreement. Therefore, in an effort to mitigate climate change, it is imperative that the global energy economy transforms from one based predominantly on the burning of fossil fuels to a low carbon economy based on energy efficiency and renewable energy. Tidal energy is a very promising energy source for the near future. Firstly, due to its inherently renewable nature which helps decarbonise society reducing environmental impact, and, secondly, due to its predictability which makes it stand out amongst some other renewable energy sources. However, the tidal energy market seems to be far from mature [1-3]. Currently, Europe has approximately 100MW of tidal stream capacity (including in the water, under construction and permitted) [4]. Manufacturers have not embraced a design standard and many different technology solutions currently appear both at structural level and operation level [5]. In this sense, a quick look at the current state of technology will identify turbines with different number of blades, hubless designs, grounded or floating solutions, and reversible or rotating unidirectional operation [6][7]. Despite this, the EU-Ocean Energy Association predicts 100GW of tidal stream power by 2050 [4].

Reducing costs and increasing performance through innovation and testing is one of the six essential priority areas identified by the European Technology and Innovation Platform for Ocean Energy (TP Ocean) to be addressed to improve ocean energy technology and decrease its risk profile [4]. In recent years, many different testing facilities have been designed/developed in line with EU vision. In this sense, facilities for scaled down systems [8][9], full scale components [10] and real sea environment [11] [12] are gaining popularity in the academic and industrial field. MaRINET2 project [13] offers a catalogue of many of these facilities. To address the need of industry and researchers, the Centre for Marine and Renewable Energy (MaREI) has developed the capability (infrastructure, personnel and knowledge) to conduct static and fatigue testing of full scale tidal turbine blades in the large structures test cell at the National University of Ireland Galway (NUI Galway). Physical testing, together with numerical modelling, has become an essential tool to

underpin design solutions and obtain critical certification for commercialisation purposes. Many different structural tests can be designed (for example, static [14], fatigue [15], dynamic [16] and modal [17]) in any of the many components of a marine energy device [10][18]. Typically, a combination of these is required to fully characterise the system.

Well-documented cases of marine renewable energy device failures resulting from material damage have highlighted the issue of reliability and the importance of adequate durability in their design. Therefore, fatigue testing should be adopted as an important tool at each design stage (material [19], component [20], subsystem and prototype) of marine energy devices due to the difficulty and cost to perform any type of maintenance operations. In fact, the purpose of fatigue testing is to study the life expectancy of the system under operating conditions by applying (cyclic) loading to it which produces equivalent damage at a faster rate [21].

1.2 Objective of study

OpenHydro's turbine underwent a significant design change in which the blades were designed to cantilever from the outer ring structure. This new blade design and blade attachment method offered a number of improvements such as increased hydrodynamic efficiency and reduced component count. To validate and de-risk this significant design change, a blade qualification programme was launched. The results of this testing were a pre-requisite for the deployment of two of the "world's first grid-connected tidal arrays" in Paimpol-Bréhat, France and the Bay of Fundy in Canada, both consisting of two 16m diameter OpenHydro turbines. Furthermore, the test results will be an important input into the next generation turbine design.

As part of the blade qualification programme, a scaled part of an OpenHydro (OH) prototype 10-blade tidal hubless turbine was tested in the Large Structures Laboratory of MaREI at NUI Galway. In the current paper, a fatigue test setup of the scaled down hubless tidal turbine subsystem in the laboratory is presented, together with some preliminary results. There were two main objectives – to validate (i) the assembly methodology of inserting the blade into the rotating ring structure and (ii) the performance of the sub-assembly under fatigue (high-cyclic) loading to confirm that the system can achieve its life expectancy under operating conditions.

2 EXPERIMENTAL SETUP

The tested subsystem consisted of a 3/8 scaled part of an OpenHydro (OH) prototype 10-blade tidal hubless turbine, which can be seen in Figure 1. In particular, one blade and a sector of the rotating ring (Figure 2) were installed in a 10m x 6m x 6m reconfigurable steel frame in the Large Structures Laboratory of MaREI at NUI Galway. A specially designed load saddle was used to load the blade when connected to the hydraulic actuator.

2.1 Instrumentation

Of particular interest was the attachment of the turbine blade to the rotating ring and, thus, a rich set of sensors were deployed to monitor the behaviour of this region within the tested subsystem. The blade was fixed to the ring sector by 8 number titanium bolts. Each of these bolts were monitored with four linear strain gauges (SG) at 0°-90°-180°-270° orientations.

The strain level in the ring was also monitored in different interesting locations on the test box (representing a section of the rotating ring) previously identified by finite element modelling (FEM) numerical simulations. High temperature SGs were used (1.5% strain limit) within the ring sector to avoid damage during welding process. Different standard SGs (linear and rosette) have also been used to monitor the strain on the blade. The standard SGs have a 5% strain limit. The displacement field was also monitored in different points; three types of sensors have been used in this test: Linear Variable Differential Transformers (LVDT) for short displacement range (up to ±25 mm, 0.1% linearity), draw-wire potentiometers for displacement of up to 1000 mm (0.1% linearity) and crack opening sensors installed between two specific points (5 mm range). A Digital Image Correlation (DIC) stereo camera device was used to capture the 3D displacement and strain fields on the rear side of the ring sector (Fig 2). As an image-based measurement, the accuracy is directly related to the field of view. In this case, a 1 m^2 was captured by both photographic cameras. The area was prepared (a stochastic high contrast pattern should be painted on the surface) and by preliminary tests a ±50 micrometres noise level was observed. A load cell was used to directly measure the loads applied by the actuator to the sub-structure. Table 1 summarises the sensors type used and their location in the subsystem.

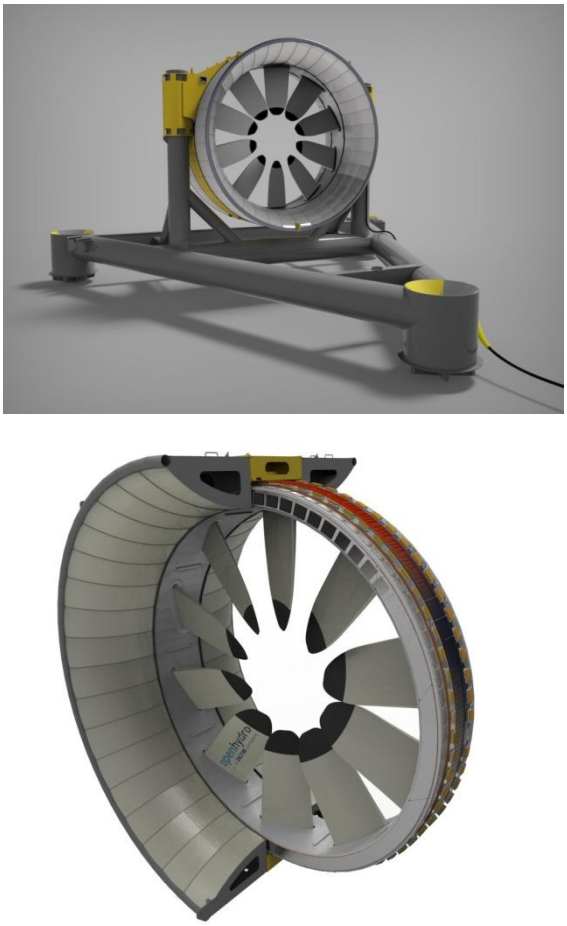

Figure 1. 3D Models of a hubless tidal turbine (top) and detail of rotating ring (bottom)

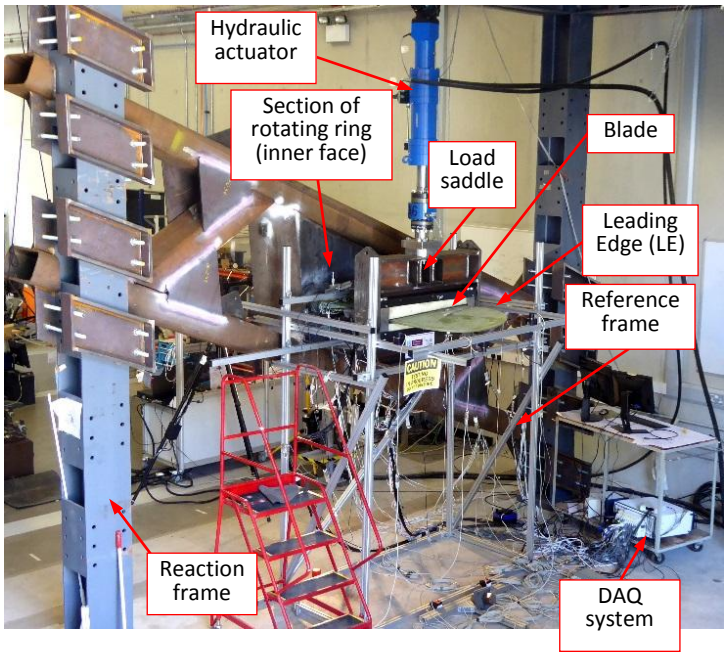

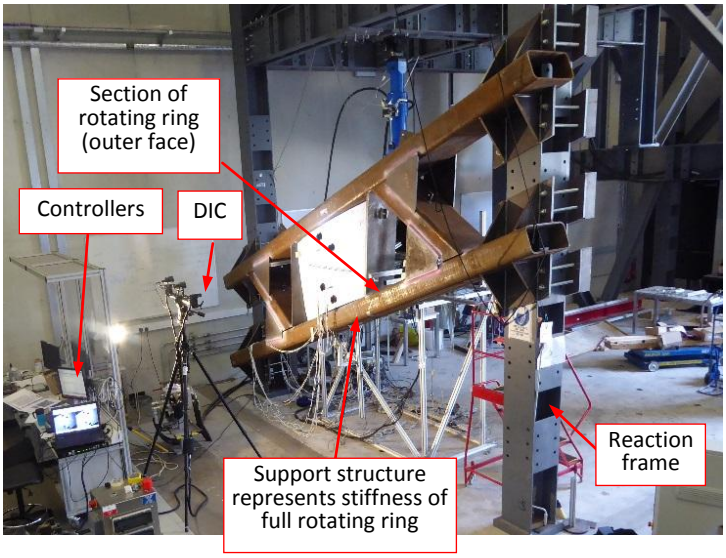

Figure 2. Tidal turbine sub-structure being tested at the National University of Ireland Galway

Measurement	*Quantity*	*Location*	*Sensor Type*
Strain	32	Bolts	Linear SG
	18	Ring Sector	Linear & Rosette SG
	33	Blade	
	1	Ring Sector	DIC
Displacement	8	Ring Sector	LVDT
	8	Blade	LVDT
	5	Blade	Draw-wire sensor
	3	Blade Ring gap	Crack Opening
	2	Frame	LVDT
	1	Actuator	LVDT
	1	Ring Sector	DIC
Load	1	Actuator	Cell Load

Table 1. Sensor number, type and location

2.2 Test characteristics

The high cycle fatigue tests were conducted under load control, where the digital controller and software ensured that the actuator automatically applied a constant load amplitude to the tested sample in each loading (± 2% of target load). Four different load amplitudes have been used through the whole test. Table 2 summarises the number of effective cycles performed at each load which were carried out sequentially. The

loading profile was chosen to represent accumulative damage expected in the turbine sub-components at the site of deployment. Figure 3 shows the displacement-load characteristics for the initial 3,600 cycles at each load amplitude.

Stage	*Number of cycles*	*Load Amplitude*	*Description*
1	225,000	±19.4 kN	100% Damage, 2.3% probability of failure
2	177,000	±25.0 kN	100% Damage, 50% probability of failure
3	101,000	±30.0 kN	Increased load to accelerate damage accumulation
4	275,000	±35.0 kN	Maximum actuator load, exceeding 100% damage, 2.3% probability of survival

Table 2. Effective cycles performed at each load stage

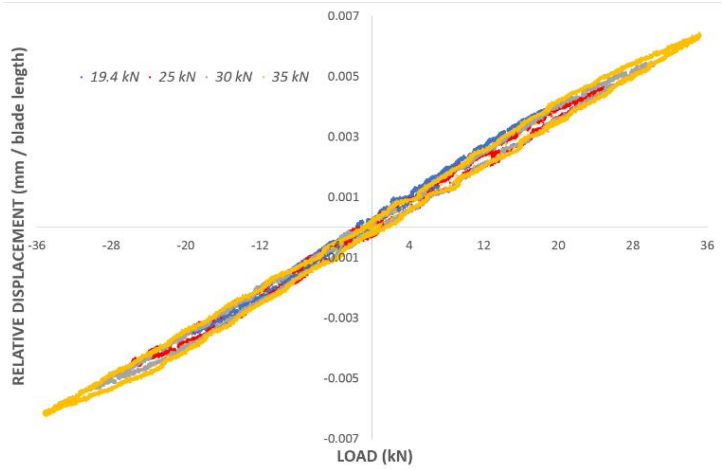

Figure 3. Vertical displacement-load characteristics for all cycles measured at the loading point.

The hydraulic actuator has a maximum capacity of ± 250 kN and 250 mm travel (Fig 2). The fatigue test was programmed using Cubus® software, where a 1 Hz sinusoidal cycle test was implemented. The controller is effectively a PID controller with user selectable constants to modify the response both in time and amplitude and adjust it better to a pure sinusoidal signal. A NI PXIe Data Acquisition system allowed synchronised readings of 110 channels and three High Definition (HD) cameras at 20 samples per second. The test was carried out through 19 effective testing days at an average working load of 12 hours/day, but was run

up to 24 hours/day non-stop. Frequent visual checks were carried out in key locations of the subsystem and the frame to assure good structural behaviour throughout the whole test.

2.3 Numerical model

The structural finite element (FE) model of the system shown in Figure was created in ANSYS Workbench® 16.1 prior to undertaking the physical tests. Its primary function was to understand the design of the test structure and assembly to the reaction frame, as well as the load transfer through the system during cycling. The load application point on the blade in the test is replicated in the model and run for the cases detailed in Table 2.

The model comprises both Solid and Shell elements. 320,000 shell elements modelled the diagonal beams, the test box and attachments. The blade and bolts have been modelled with 690,000 solid elements. A static structural analysis was carried to observe the blade general deflection field under the different loads shown in Table 2.

A detailed comparison of the numerical model to the physical experiment is beyond the scope of this paper and as such will not be described here. The primary function of the FE model in this analysis was to check the global response of the system to the input loads for comparison during the test. The numerical model was not intended to capture all of the phenomena observed in the physical test (it was prohibitive to run the model for the same number of cycles expected in the test and long term behavior of the system could not be accurately captured to the detail observed in the test). Additional work is required to fully understand the comparison between the experimental and numerical results and will be the subject of future investigations.

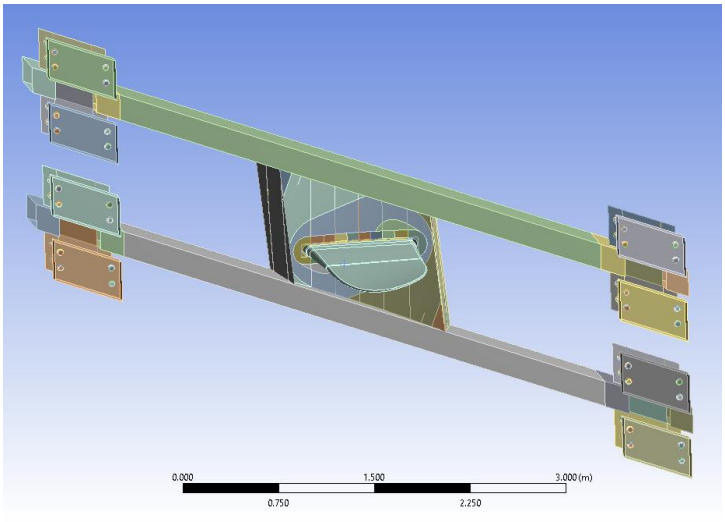

Figure 4. Overview of geometry modelled in ANSYS FE. Reaction frame support members removed for clarity.

3 RESULTS

This results section details two separate stages of the test program, both of which were critical to further understand the behaviour of the attachment system solution (blade-rotating ring). Specifically, that is, to (i) validate the blade insertion methodology and (ii) investigate the performance of the sub-assembly under fatigue load to validate previously developed numerical models.

3.1 Blade insertion

The goal of this phase was to have the blade sufficiently secured into the sector of the rotating ring with the position of the blade being maintained by a combination of the clamping effect of the structure and pretension in the attachment bolts. The insertion metric used to determine the final position were predetermined strains local at the slot opening in the rotating ring structure that the blade was inserted into. These strain values were known from a finite element (FE) model (not detailed in this paper) to correspond to the required blade position. Equalising these local strains was also expected to maintain an even clamping force on the blade and load transfer through the structure. This strain is shown in Figure 5, which is normalised relative to the yield strain of the material.

The opening of the blade slot during this process (Figure 6) also illustrated this effect with a consistent opening of both the leading (LE) and trailing edges (TE) of the blade slot (the blade and blade slot are tapered and as such a slight opening of the structure as the blade is inserted is to be expected).

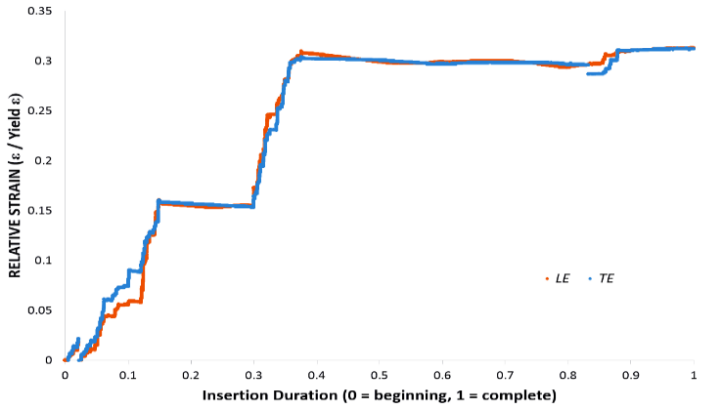

Figure 5. Local strains monitored on the inner face of the ring sub-structure adjacent to the blade slot during insertion to ensure correct final position

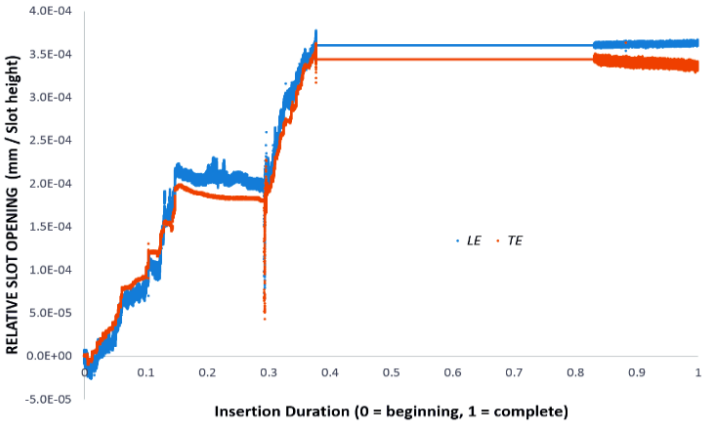

Figure 6. Opening of slot during blade insertion

In contrast to this, a distinct difference in the blade travel at the leading and trailing edges was observed during the insertion phase (Figure 7), with the leading edge travelling further into the slot than at the trailing edge. Manufacturing tolerance on both the blade and slot surfaces will account for some of this; however, this is exaggerated by the fact that the initial blade position during the insertion was not rigorously controlled and the blade would not have been perfectly aligned with the blade slot before the insertion phase was initiated. Nonetheless, it was visually evident that there was non-symmetrical travel of the blade. This also led to the conclusion that there was a slight, but still appreciable, difference in the clamping force exerted onto the blade at the extreme ends of the slot, which also had the possibility to affect the response of the blade under load.

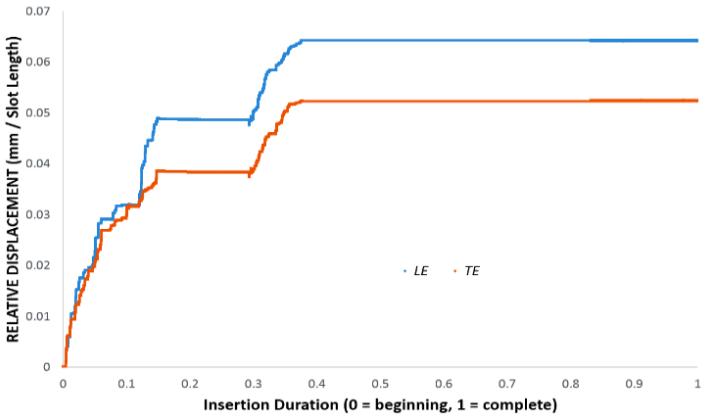

Figure 7. Blade travel during the insertion stage

Figure 8 presents the average bolt strain during the insertion phase for two bolts as an example, where Bolt 5 and Bolt 8 are close to the TE and LE, respectively. As the blade travels through the slot, it has to overcome the static friction between the blade and slot. Hence, there are instantaneous peak of strain in the bolts as they are tensioned. This results in a "stick-slip" type behaviour. Similar to the local strains in the rotating ring sub-structure adjacent to the slot, a final bolt tension (with corresponding strain) was required upon completion of the insertion process to ensure correct anchoring of the blade into the structure. This proved a challenge to achieve equally for all of the bolts, as in order to achieve pure tension, perfect geometry of the blade, bolt and slot are required, which was impossible to achieve in the test setup, and is representative of the actual turbine structure during assembly. As a result, there is a variance in the average bolt strain (Figure 8) due to slight bending being present, which affected the final values. The effect of this bending present on the bolts under cyclic load is beyond the scope of this current analysis and will be detailed in future investigations.

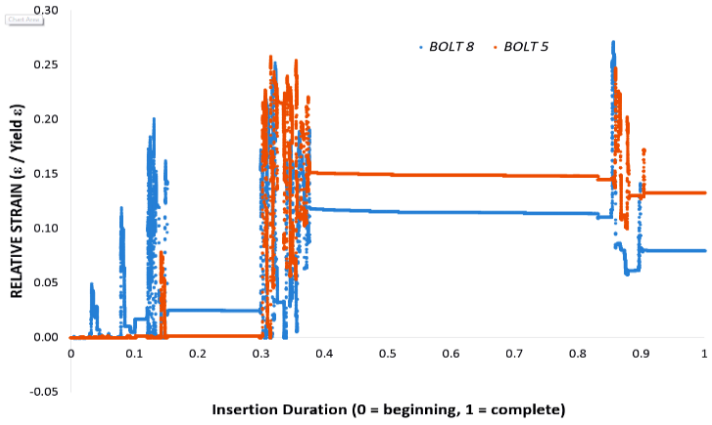

Figure 8. Average bolt strains during the insertion phase

3.2 High-cycle fatigue testing

During the fatigue test, specific attention was given to the behaviour of the ring sector and the performance of the bolted connection. Therefore, this section has been divided accordingly to present the results.

3.2.1 Structural integrity of ring sector

Internal ribs in the ring sector were monitored with SGs. The long-term effect is analysed by obtaining the average strain over 3600 cycles and plotting these for the full life cycle of the test. This way, we can observe if there is a particular trend through the whole duration of testing. Figure 9 shows the behaviour of 8 internal SGs.

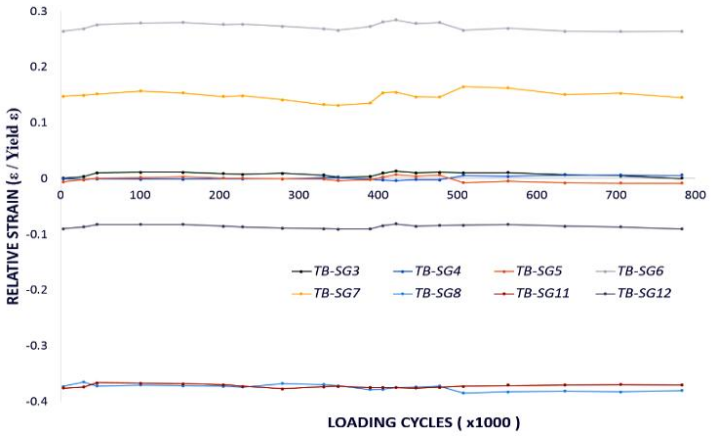

Figure 9. Averaged strain behaviour for SGs placed internally in the test box (i.e. section of the ring)

As observed, there is no significant change in the measured strains with increased number of cycles. This suggests that no significant damage occurred in the internal ribs or internal welds. This was verified by visual observations. Figure 10 shows analogous results for SGs placed on the external surface of the ring sector. There is a significant change in strain at 500,000 cycles, which can be explained by the fact that some modifications to the test box were conducted (that is, holes for visual access to internal welds were enlarged).

In the short term (behaviour during a loading cycle), the rotating ring shows an unsymmetrical behaviour. In this sense, DIC proved to be a very interesting tool, as it showed the full displacement field of the rear side of the ring. Figure 11 shows a colour map of the ring sector at two different load steps, which was obtained using the DIC system.

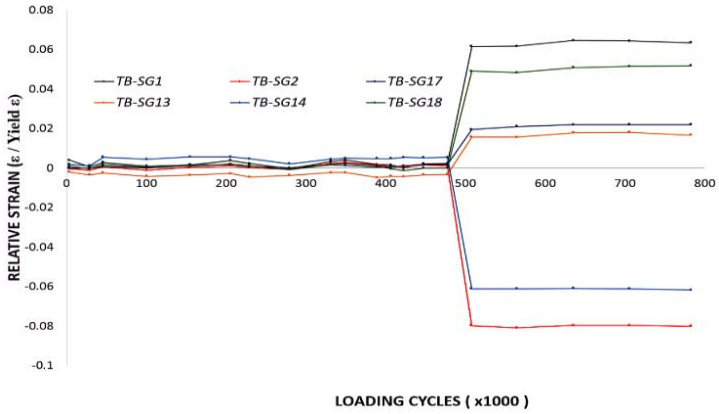

Figure 10. Averaged strain measured by SGs placed externally on the test box (ring sub-structure)

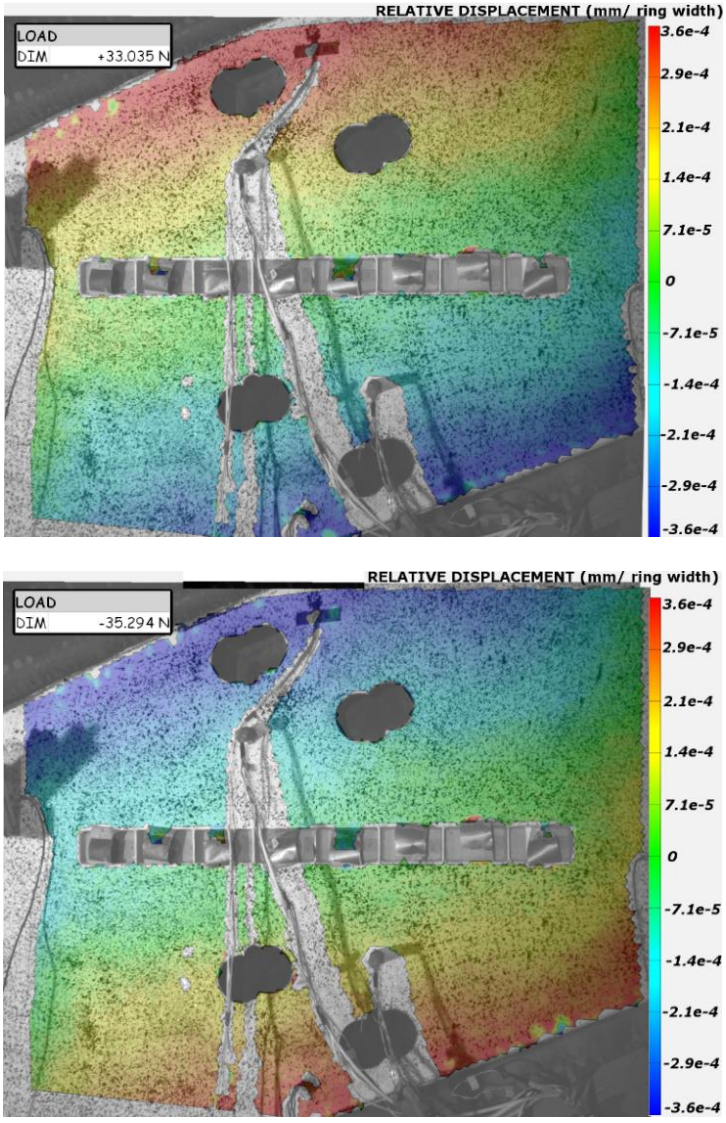

Figure 11. Out-of-the-plane displacement colour map of the outer face of the steel ring sub-structure at + 33 kN (top) and at - 35 kN (bottom) [black areas are observation holes]

In general, the upper half of the ring sector experiences larger deformations than the lower half. As expected, when the actuator pulls up the blade, the upper half moves towards the sensor and vice versa. It is interesting to observe the null movements area shape: crossing the bolts line (in the middle of the pictures) and moving towards the same diagonal corner which is where the welding points are.

The inner face of the ring sector was monitored with two LVDTs in the out-of-plane direction at the upper half and the lower part (Figure 12). The results are consistent both in magnitude and direction with those obtained from DIC (Figure 11). As observed, the upper half (orange signal) experiences larger deformations than the lower half (blue) and their movement is 180° out of phase.

3.2.2 Structural integrity of the bolted connection

After blade insertion, special attention was given to the bolted connection to understand its performance under cycling load. In this sense, the displacement measurements on the blade and the strain both in the bolts and on the inner face of the ring sector adjacent to the slot were used to draw a clearer picture of its behaviour.

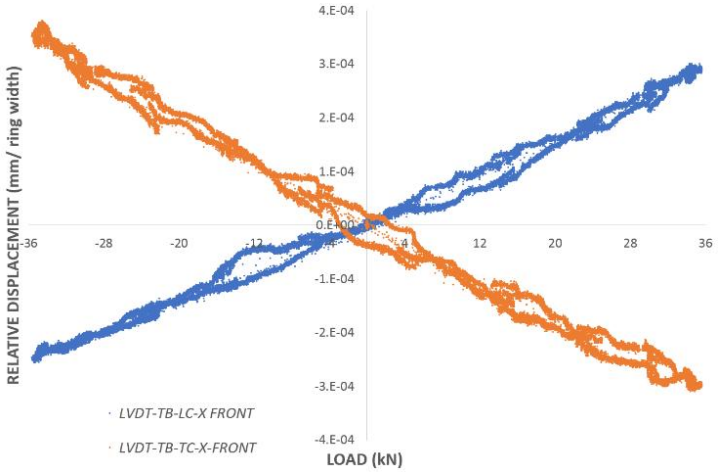

Figure 12. Out-of-the plane displacement load diagram for the ring sub-structure at ±35 kN [TB=test box; LC = lower corner; TC = top corner]

The strains in the rotating ring sub-structure adjacent to the slot measured during the whole test are plotted in Figure 13. This way, the clamping force can be monitored over the testing cycles. As observed, the averaged strain decreased at both sides of the slot during the whole duration of the high-cycle fatigue test.

Starting from initial values consistent with those shown in Figure 5, the tension strain reduced up to 16% and 13% in the LE and TE, respectively. This suggests that the clamping pressure on the blade is being reduced with increase in number of cycles during fatigue testing, which could be due to the blade moving outwards of the blade slot in the ring sub-structure (both blade and blade slot are tapered) or wear on component parts of the system during cyclic loading. Some of the reasons for this phenomenon can be investigated further by focussing on the response over a shorter duration, which can be used to highlight differences in the experimental setup or the behaviour. Figure 14 shows the strain behaviour during 10 loading cycles of the same SGs.

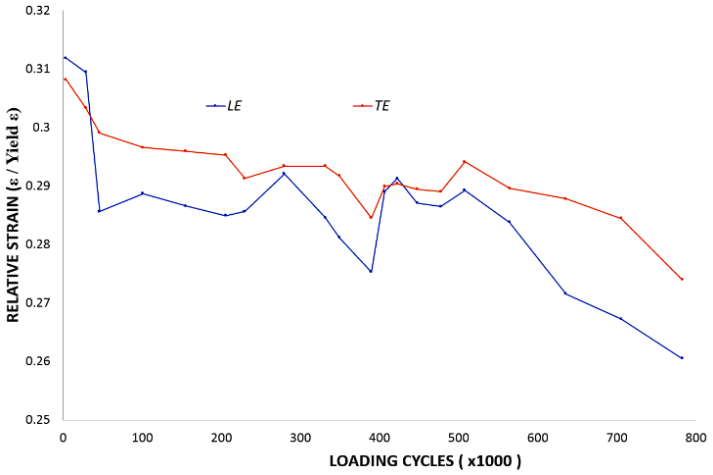

Figure 13. Averaged strains on the inner face of the ring sub-structure adjacent to the slot measured using SGs

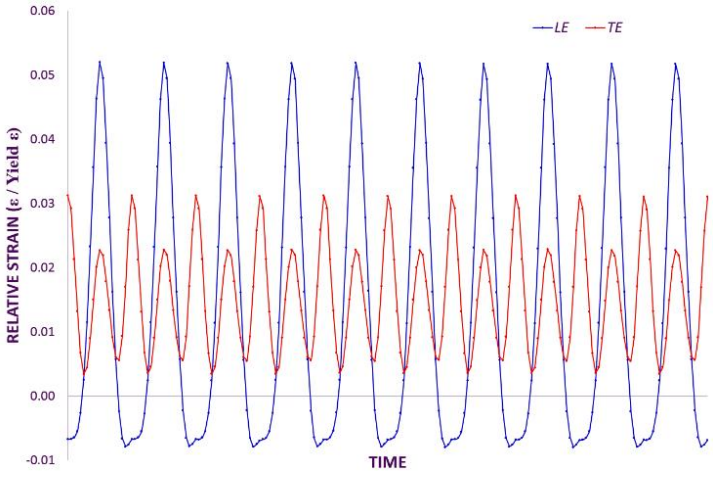

Figure 14. Strain values for the inner face of the ring sub-structure adjacent to the slot during 10 cycles at ±35 kN

It is clear that the ring sub-structure is not experiencing symmetrical strains during the loading cycles. During the whole loading cycle, the strain gauge on the inner face of the ring sub-structure adjacent to the slot

at the TE is measuring positive (tension strains). As the blade is pushed downwards by the actuator (i.e. negative load), the top of the blade reacts against the top face of the slot in the ring sub-structure that accommodates it, thus forcing the slot to open further causing increased tensile strains in the ring sub-structure adjacent to the slot (see left hand side of Figure 15 for the TE). Conversely, when the blade is pulled upwards by the actuator (i.e. positive load), the bottom of the blade reacts against the bottom face of the slot in the ring sub-structure that accommodates it, thus also forcing the slot to open further causing increased tensile strains in the ring sub-structure adjacent to the slot (see right hand side of Figure 15 for the TE). On the other hand, the strain measurements on the inner face of the ring sub-structure adjacent to the slot at the LE is suggesting that this phenomenon only happens when the blade is being pulled up by the actuator (see right hand side of Figure 15 for the LE). Considering Figure 15 (and assuming that the measurements from the strain gauge are offset due to some tensile strain not being accounted for due to setting the zero value of the gauges after some tensile strain was present), pushing down on the blade with the actuator seems to make the blade move outward from the blade slot in the ring sub-structure at the leading edge (LE).

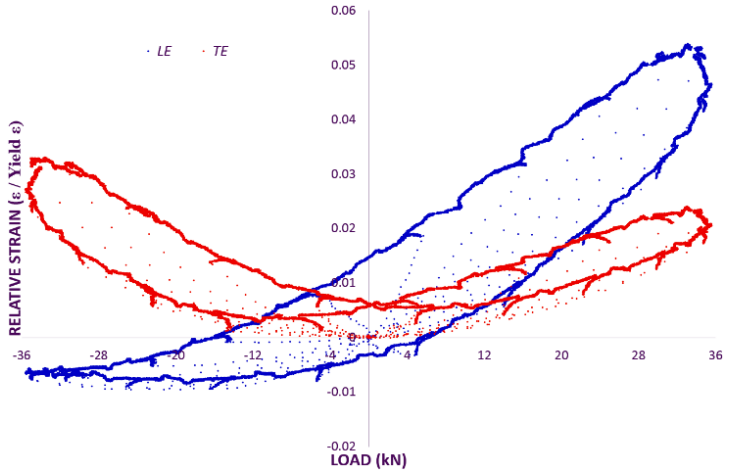

Figure 15. Strain-load graph for the inner face of the ring sub-structure adjacent to the slot during the first 3600 cycles at ±35 kN

As observed in Figure 15, the LE dissipates more energy during loading cycles than TE (fatter loop), which could indicate larger movement on that side. To further study this phenomenon, an axial travel- load plot for the blade is included in Figure 16. Figure 16 shows larger axial displacements in the LE when the

blade is both pulled up (positive load) and pushed down (negative load), which are consistent with the strain results presented in Figure 15. However, in the vertical direction, the displacements of both sides are more similar (Figure 17). Larger relative vertical displacements are observed when the blade is pulled up than when it is pushed down.

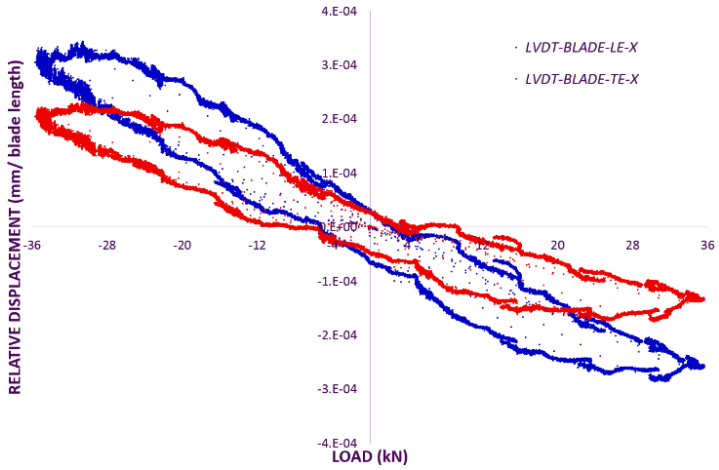

Figure 16. Relative axial displacement of the blade during the first 3600 cycles at ±35 kN

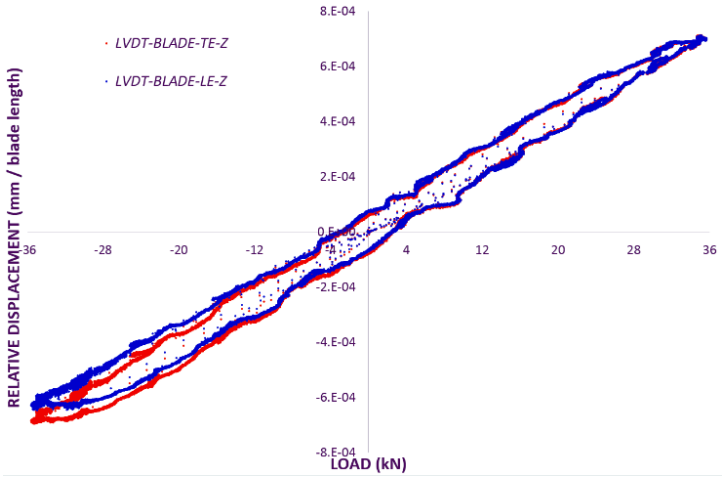

Figure 17. Relative vertical displacement of the blade close to its roots during the first 3600 cycles at ±35 kN

As can be seen from Figure 18, lateral displacement of the blade at its tip is consistent with Figures 16 and 17. Also, as observed in Figure 18, when the blade is pulled up the blade moves towards the LE and vice versa, which means that the actual load vector is applied slightly away from the neutral axis of the blade (towards the LE).

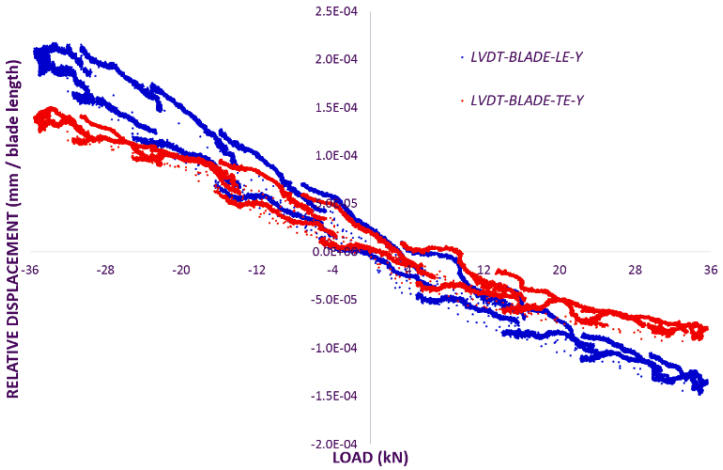

Figure 18. Relative lateral displacement of the blade close to its root during the first 3600 cycles at ±35 kN

The bolts are a very interesting location to analyse the load transfer through the system. If two bolts are selected, one close to the leading edge (Bolt 8) of the blade and one close to the trailing edge (Bolt 5) of the blade (with the same orientation), we can study differences in load transfer. When loading the system, SG1 (0°) and SG3 (180°) should show a similar behaviour, as they are just 180° out of phase. Figure 19 shows strain-load diagrams for these SGs.

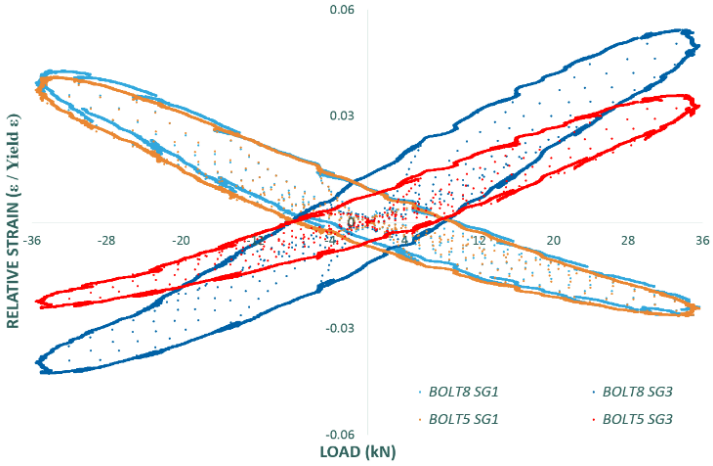

Figure 19. Strain-load diagram for Bolt 8 and Bolt 5 at 0° (SG1) and 180° (SG3) during the first 3600 cycles at ±35 kN

SG1s behave similarly at both sides (LE and TE). However, the lower part of Bolt 8 at the LE side experiences higher strains (in absolute values, measured by SG3) than the equivalent part of Bolt 5 at the TE, both when compressed and when extended. Overall, the behaviour is not as symmetric as it would have been

planned, but consistent with what has been observed from the strain gauge measurements on the inner face of the ring sector (Figure 15) and the axial blade movement (Figures 16). In other words, it suggests that there is a lower clamping force on the LE side and, thus, there is increased movement of the blade in the slot on the LE side (according to Figure 16) and the bolts on the LE (e.g. Bolt 8) are experiencing some bending, whereas the blade is relatively well clamped on the TE and so the bolts don't experience any significant bending.

SG2s and SG4s lay on the plane defined by the blade's surface. Theoretically, if the loading vector is vertical, these SGs should keep their tension constant through a loading cycle. As observed in Figure 20, SGs located on Bolt 5 in the TE behave close to what was expected. They stay in tension during the whole loading cycle. SG2 on Bolt 8 in the LE experiences larger positive strain when the blade is pulled up, which is consistent with larger lateral deflections found in the blade (Figure 18) and when it is pushed down, it goes into compression. This behaviour seems to confirm a slight vertical misalignment in the loading vector and a lower clamping force present on the LE.

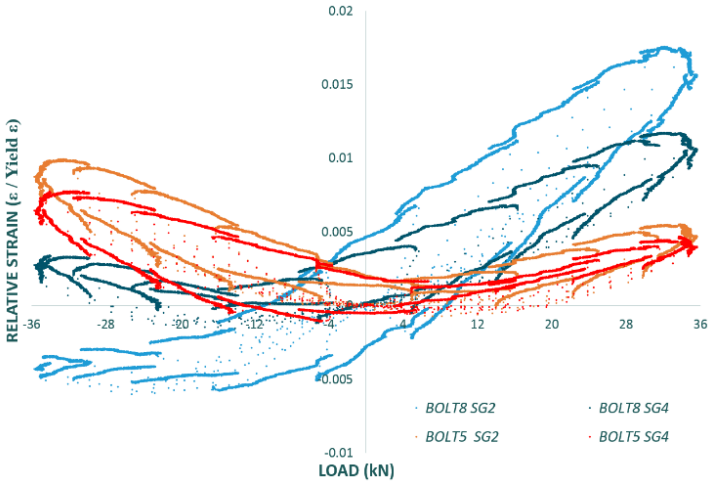

Figure 20. Strain-load diagram for Bolt 8 and Bolt 5 at 90° (SG2) and 270° (SG4) during ±35 kN cycles

3.3 Numerical modelling

In general, the FE model shows good agreement with the test results when the global response of the structure (total blade deformation) is considered (Table 3). A similar deformation shape was observed (see Figure 21).

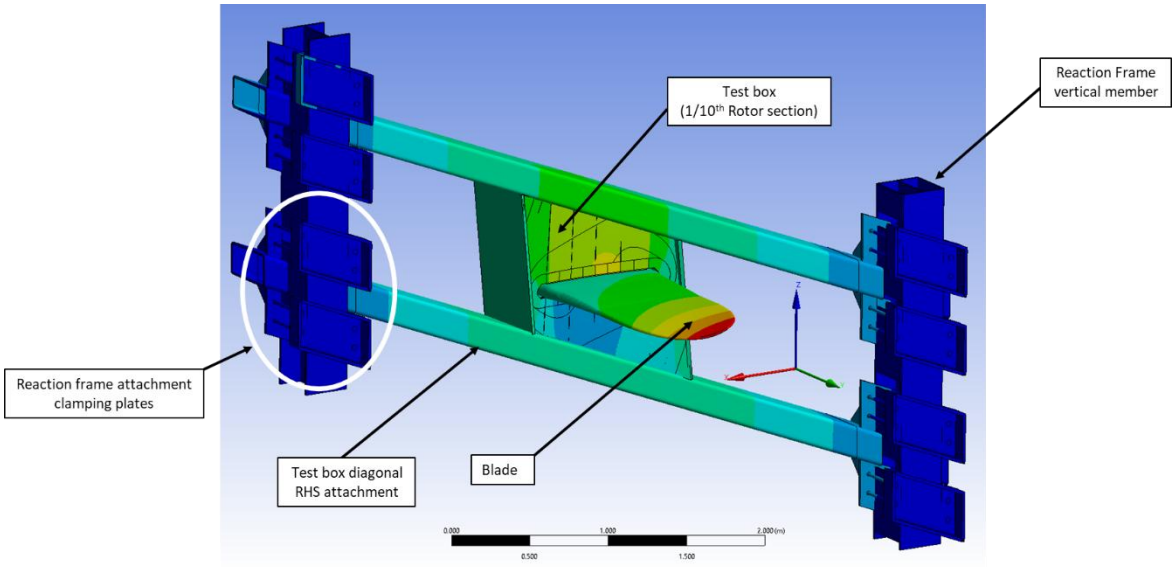

Figure 21. Total Deflection for Load Case 1 (19.4kN) with red colour representing maximum values (3.16e-3 normalised deflection)

Of interest to note is how the difference between the values increases slightly with the load application. This phenomenon may not be fully attributable to a difference in blade load, however, as when the 30kN load was applied during the test, approximate 500,000 cycles had been put through the system which was not accounted for in the FE model. A similar observation may be considered for the 35kN load case. This further highlights the need to fully understand the response of the blade and blade slot under the cycle accumulation before attempting a thorough analysis of the comparison between the numerical model and experimental data, which is outside the scope of this paper.

Load Case	**19.4 kN**	**25 kN**	**30 kN**	**35 kN**
FE Model	3.16e-3	3.66e-3	4.47e-3	5.35e-3
Test	3.23e-3	3.55e-3	4.15e-3	5.09e-3
% Difference	-2.3%	3.0%	7.1%	4.9%

Table 3 Normalised blade deflection for various load cases considered in FE model and high-level comparison with physical test data

4 DISCUSSION AND CONCLUSIONS

Outcomes of the overall test programme of a tidal turbine blade sub-assembly are: validating the installation process (including potential improvements for future turbine designs), improving the device structural design and bringing down the levelized cost of energy (LCOE) for the turbines. The analysis presented in this paper represents a significant contribution toward reaching those goals. It has also resulted in the hardware-software systems for testing, as well as expertise, being developed in the MaREI Large Structures Testing facility at NUI Galway.

More specially, in relation to the performance of the tidal turbine sub-assembly, the structural integrity of the ring steel substructure was proven with no signs of damage or failure to the plates or weld within the ring steel substructure during the accelerated life study that represented the loading history of the blade under operational conditions for a typical turbine deployment life. The structural integrity and performance of the tested subsystem has not showed any significant change as shown in the long-term averages over the duration of the test. Thus, the ring sub-structure was found to perform satisfactorily under equivalent life high cycle fatigue loading.

It is evident from the high cycle fatigue tests that there was non-symmetrical behaviour of the connection of the blade to the ring that was not fully appreciated before the testing occurred and was an important learning outcome. This was attributed to a difference in the clamping of the blade on either side of the slot by the ring sub-structure. The impact of this finding on a full tidal hubless system needs further investigation, as part of the reason for this phenomenon may have been due to the method that was employed in the laboratory of load transfer from the hydraulic actuator to the blade element through a clamping load saddle.

ACKNOWLEDGEMENTS

The authors would like to acknowledge the support of Science Foundation Ireland through the National Centre for Marine and Renewable Energy Ireland (MaREI) (Grant no. 12/RC/2302). The authors would also like to acknowledge Mr Colm Walsh for his support and contribution during the testing campaign. The last

author would also like to acknowledge the support of Science Foundation Ireland through the Career Development Award programme (Grant no. 13/CDA/2200).

REFERENCES

[1] A. Badcock-Broe, R. Flynn, S. George, R. Gruet and N. Medic, "Wave and Tidal Energy Market Deployment Strategy for Europe," Strategic Initiative for Ocean Energy, 2014.

[2] Transparency Market Research, "Wave and Tidal Energy Market- Global Industry Analysis, Size, Share, Growth, Trends and Forecast 2016-2024," 2016.

[3] Ocean Energy Forum (2016). "Ocean Energy Strategic Roadmap 2016, building ocean energy for Europe".

[4] Magagna D, Monfardini R, Uihlein A. JRC "Ocean Energy Status Report: 2016 Edition EUR 28407 EN". Luxembourg (Luxembourg): Publications Office of the European Union; 2016. JRC104799

[5] P. Fraenkel, "Practical tidal turbine design considerations: a review of technical alternatives and key design decisions leading to the development of the SeaGen 1.2MW tidal turbine", Proceedings- Fluid Machinery Group- Ocean Power Fluid Machinery Seminar, Institution of Mechanical Engineers, London, 2010.

[6] I.S. Hwang, Y.H. Lee and S.J. Kim, "Optimization of cycloidal water turbine and the performance improvement by individual blade control", Applied Energy, 86, 1532-1540, 2009.

[7] Electric Power Research Institute (EPRI), "Tidal in stream energy conversion (TISEC) devices – survey and characterization". EPRI North American Tidal in stream energy conversion feasibility demonstration project, 2005.

[8] P. Jeffcoate, T. Whitakker, C. Buake and B. Elsaesser, "Field tests of multiple 1/10 scale tidal turbines in steady flows", Renewable Energy, vol 87, Part 1, p240-252, 2016.

[9] T. Vyzikas, S, Deshoulieres, M. Barton, O. Giroux, D. Greaves and D. Simmonds, "Experimental Investigation of different geometries of fixed oscillating water columns", Renewable Energy, vol 104, p248-258, 2017.

[10] P. Thies, L. Johanning, K.A. Karikari-Boateng, C. Ng and P. McKeever, "Component reliability test approaches for marine renewable energy". Proceedings of the Institution of Mechanical Engineers, Part O: Journal of Risk and Reliability 229(5):403–416, 2015.

[11] B. Sellar, G.Wakelam, D. Sutherland, D. Ingram and V. Venugopal, "Characterisation of Tidal Flows at the European Marine Energy Centre in the Absence of Ocean Waves", Energies, 2018.

[12] E. Cullen, R. Chumbinho and J. Breslin, "SmartBay Ireland's marine real time data acquisition system", DOI**:** 10.1109/OCEANS.2014.7003264 . 2014 Oceans Conference, Canada.

[13] MaRINET2 project, "Leading Access to Marine Research Facilities", 2017 [Online]. http://www.marinet2.eu/

[14] D. Miller, J.F. Mandell and D. Samborsky, "Evaluating Performance of Composites Materials for MHK Applications", Proceedings of the ASME Int. Mechanical Engineering Congress & Exposition, Colorado, USA, 2011.

[15] J.F. Mandell, D. Samborsky and P. Agastra,"Composite Materials Fatigue Issues in Wind Turbine Blade Construction", SAMPE, 2008.

[16] G. Crammond, S.W. Boyd and J.M. Dulieu-Barton,"Dynamic analysis of composite marine structures using full-field measurement techniques", Journal of Marine Engineering & Technology,13:1, 23-35, 2014.

[17] D.T. Griffith and T.G. Carne, "Experimental Modal Analysis of 9-meter Research-sized Wind Turbine Blades", Proceedings of the IMAC XXVIII, Florida, USA, 2010.

[18] I.M.L. Ridge, "Tension-torsion fatigue behaviour of wire ropes in offshore moorings", Ocean Engineering, vol 36, p650-660, 2009.

[19] K.A. Karikari-Boateng, "Accelerated testing of tidal turbine main bearing in a full scale nacelle test rig", University of Exeter, PhD Thesis, 2016.

[20] C.R. Kennedy, S.B. Leen and C.M.Ó. Brádaigh,"Inmersed Fatigue Perfomance of Glass Fibre-Reinforced Composites for Tidal Turbine Blade Applications", Journal of Bio- and Tribo- Corrosion, 2:12, 2016.

[21] P. Brondsted and R.P.L. Nijssen, "Advances in wind turbine blade design and materials. Chapter 14: Wind turbine blade structural performance testing", Woodhead Publishing, 2013.